Large Scale MOCVD Synthesis of Hollow ReS_2 Nanoparticles with Nested Fullerene-Like Structure

Aswani Yella, Helen Annal Therese, Nicole Zink, Martin Panthöfer, and Wolfgang Tremel*

Institut für Anorganische Chemie und Analytische Chemie der Johannes Gutenberg-Universität, Duesbergweg 10-14, D-55099 Mainz, Germany

Received October 25, 2007. Revised Manuscript Received February 5, 2008

The synthesis of ReS_2 onionlike nanoparticles by means of a high-temperature MOCVD process starting from $Re_2(CO)_{10}$ and elemental sulfur is reported. The reaction is carried out in a two-step process where the intermediate product, amorphous ReS_2 nanoparticles, formed through the high-temperature reaction of rhenium and sulfur in the initial phase of the reaction, are isolated and converted into onion-type ReS_2 nanoparticles in a separate annealing step. Analysis of the reaction product using X-ray diffraction (XRD) and high-resolution transmission electron microscopy (HRTEM) combined with energy-dispersive X-ray spectroscopy (EDX) allowed us to optimize the reaction in such a way that only onionlike structures are formed.

Introduction

Early transition metal chalcogenides MQ_2 (M = group 4−7 metal; Q = S, Se, Te) adopt a characteristic layered structure. MQ_2 slabs are formed by two layers of close-packed chalcogenide atoms sandwiching one layer of metal atoms in between. These slabs are stacked, with only van der Waals forces between them.[1] Their layered nature makes these compounds excellent solid lubricants.[2] The metal coordination may vary depending on M: group 4, 5, and 7 metals prefer octahedral coordination geometry, whereas a trigonal prismatic coordination is adopted by the group 6 metals Mo and W. For example, the trigonal prismatic metal coordination is directly related to the semiconducting properties of MoS_2 and WS_2.[3,4] On the other hand, the clustering distortion observed in crystalline ReS_2 is associated with the d^3 electron count of the octahedrally coordinated transition metal.[5] As far as reactivity is concerned, sandwiching of the metal atoms between the chalcogenide layers sterically shields the metal atoms from the reaction with oxygen, which makes layered chalcogenides inert even in moist air at temperatures close to 100 °C.[6] This adjustable reactivity makes them interesting materials in the fields of catalysis or solid lubrication.[7]

In analogy to nested carbon fullerenes[8] and nanotubes,[9] Tenne and co-workers discovered related MQ_2-based (M = early transition metal, Q = S, Se) concentric closed-shell materials which triggered an avalanche in the entire field of nanostructures based on inorganic materials.[10,11] Although fullerene-type nanoparticles, nanopolyhedra, and nanotubes represent an integral part of the phase diagram of MQ_2[12] they are metastable at room temperature. High preparation temperatures (>800 °C) are needed in order to interconnect the edges of single MQ_2 layers through the formation of rhomboidal and triangular point defects which provide curvature to the otherwise flat 2D MQ_2 slabs. A key problem in the synthesis of MQ_2 fullerene-type nanoparticles and nanotubes in bulk quantities is that they are high-temperature and low-pressure phases in the M−Q diagrams, which are not accessible by traditional solid-state synthesis. In conventional high-temperature reactions, the energy required for the solid-state diffusion of the reactants would exceed the nucleation energy of metastable MQ_2 nanoparticles. As a consequence, only the thermodynamically stable crystalline products are formed. In contrast, reactions are kinetically controlled when solid-state diffusion plays only a minor role. Here a phase may nucleate and grow until its growth exhausts the supply of the reactants. Now, the sequence of phases formed depends on their relative activation energies of nucleation.

In fact, all reported synthetic approaches to onion-type chalcogenide nanoparticles such as arc discharge,[13,14] sul-

* Corresponding author. Tel: (49) 6131-39-25135. Fax: (49) 6131-39-25605. E-mail: tremel@uni-mainz.de.

(1) Tenne, R. *Angew. Chem., Int. Ed* **2003**, *42*, 5124–5132.
(2) (a) Rapoport, L.; Bilik, Y.; Feldman, Y.; Homyonfer, M.; Cohen, S. R.; Cohen, R.; Tenne, R. *Nature* **1997**, *387*, 791–793. (b) Chhowalla, M.; Amaratunga, G.A. J. *Nature* **2000**, *407*, 164–167.
(3) Tremel, W.; Seshadri, R.; Finckh, E. W. *Chem. Unserer Zeit* **2001**, *35*, 42–58.
(4) Tremel, W.; Finckh, E. W. *Chem. Unserer Zeit* **2004**, *38*, 326–339.
(5) Kertesz, M.; Hoffmann, R. *J. Am. Chem. Soc.* **1984**, *106*, 3453–3460.
(6) Ross, S.; Sussman, A. *J. Phys. Chem.* **1955**, *59*, 889–892.
(7) (a) Afanasiev, L.; Rawas, L.; Vrinat, M. *Mater. Chem. Phys.* **2002**, *73*, 295–300. (b) Mdleleni, M. M.; Hyeon, T.; Suslick, K. S. *J. Am. Chem. Soc.* **1998**, *120*, 6189–6190. (c) Bollinger, M. V.; Lauritsen, J. V.; Jacobsen, K. W.; Norskov, J. K.; Helveg; Besenbacher, S. F. *Phys. Rev. Lett.* **2001**, *87*, 196803–1.
(8) Kroto, H. W.; Heath, J. R.; O'Brien, S. C.; Curl, R. F.; Smalley, R. E. *Nature* **1985**, *318*, 162–163.
(9) Chopra, N. G.; Luyken, R. J.; Cherrey, K.; Crespi, V. H.; Cohen, M. L.; Louie, S. G.; Zettl, A. *Science* **1995**, *269*, 966–967.
(10) Tenne, R.; Margulis, L.; Genut, M.; Hodes, G. *Nature* **1992**, *360*, 444–446.
(11) Feldman, Y.; Wasserman, E.; Srolovitz, D.; Tenne, J. R. *Science* **1995**, *267*, 222–225.
(12) Margulis, L.; Salitra, G.; Tenne, R.; Talianker, M. *Nature* **1993**, *365*, 113–114.
(13) Chhowalla, M.; Amaratunga, G. A. J. *Nature* **2000**, *407*, 164–167.

10.1021/cm7030619 CCC: $40.75
Published on Web 05/15/2008

furization/selenisation of metal oxides,[15,16,17–25] chlorides[26,27] or carbonyls,[28] decomposition of ammonium thiometallates,[29–32] chemical vapor transport,[33,34] laser ablation,[35–38] microwave plasma,[39,40] atmospheric pressure chemical vapor deposition (APCVD),[26,41] and spray pyrolysis[42] rely on the minimization of solid-state diffusion. Recently, the coffee-stain effect, a classical phenomenon in surface chemistry,[43] was applied to explain the formation of hollow spherical inorganic particles.[44] Although the experimental demonstration and theoretical treatment of this effect is concerned mostly with capillary flow and diffusion on surfaces, the general fabrication route provided by this effect seems to be applicable in a more general sense for the morphosynthesis of inorganic and organic materials. In this contribution, we report a facile large-scale synthesis of hollow inorganic fullerene (IF)-like ReS_2 nanoparticles, by suppressing solid-state diffusion through a metal organic chemical vapor deposition (MOCVD) approach. Hollow particles IF-type ReS_2, a layered metal chalcogenide, are formed because of a 3D analogue of the coffee-stain effect.

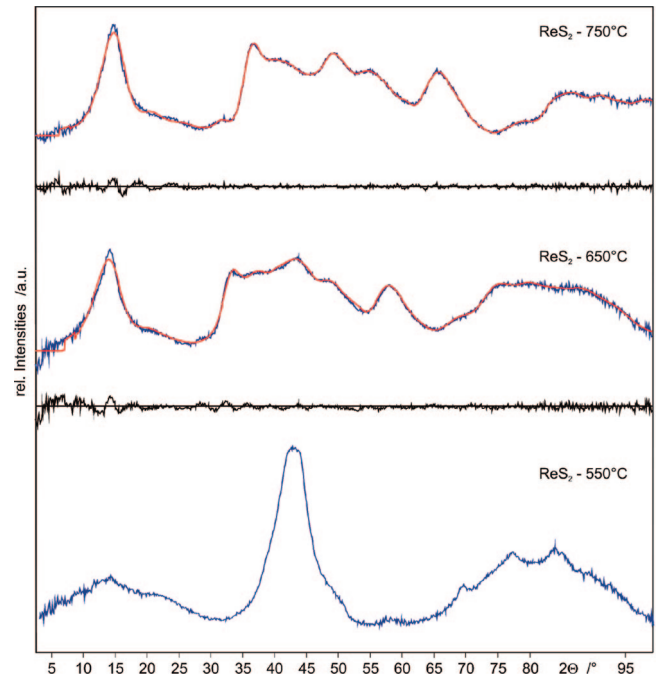

Figure 1. XRD patterns (blue, experimental; red, calculated; black, difference curve) of the samples synthesized at 550, 650, and 750 °C.

Experimental Section

Synthesis of IF-ReS_2. IF-ReS_2 was synthesized using conditions similar to those employed for the synthesis of IF-MoS_2.[45] First, a MOCVD synthesis (e.g., at 750 °C, reaction time 2 h) was carried out and the resulting material, collected from the inner walls of the small glass cylinder, was subjected to thermal annealing (e.g., at 800 °C for 1 h under Ar) in a conventional tube furnace.

A more detailed description of the setup is given in Etzkorn et al.[45] While the precursors $Re_2(CO)_{10}$ and S were heated at 210 and 250 °C, respectively, in all experiments, the temperature of the hot reactor zone was varied from 650 to 850 °C in steps of 100 °C for different sets of experiments. A constant reaction time of 2 h was used for the MOCVD step in all experiments.

In a typical MOCVD run, 0.150 g of $Re_2(CO)_{10}$ (Aldrich, 99%) and 0.256 g of S (Alfa Aesar, 99,5%+, −100 mesh, sublimed) were weighed in and inserted into the setup under constant Ar flow. Prior to the synthesis, the setup was flushed with Ar for at least 30 min. Subsequently, the graphite receptor was heated to the desired reaction temperature (temperature at the graphite receptor (T_{ind}) = 550, 650, 750, and 850 °C respectively) by induction. Once the appropriate reaction temperature was reached, the precursors were heated. The heating rates were

(14) Hu, J. J.; Bultman, J. E.; Zabinski, J. S. *Tribol. Lett.* **2004**, *17*, 543–546.
(15) Camacho-Bragado, G. A.; Elechiguerra, J. L.; Olivas, A.; Fuentes, S.; Galvan, D.; Yacaman, M. J. *J. Catal.* **2005**, *234*, 182–190.
(16) Chen, W. X.; Tu, T. P.; Ma, X. C.; Xu; Tenne, Z. D.; Rosenstveig, R. *Chin. Chem. Lett.* **2003**, *14*, 312–315.
(17) Feldman, Y.; Frey, G.; Homyonfer, M.; Lyakhovitskaya, V.; Margulis, L.; Cohen, H.; Hodes, G.; Hutchison, J. L.; Tenne, R. *J. Am. Chem. Soc.* **1996**, *118*, 5362–5367.
(18) Feldman, R.; Margulis, L.; Homyonfer; Tenne, M. R. *High Temp. Mater. Proc.* **1996**, *15*, 163–169.
(19) Feldman, R.; Zak, A.; Popovitz-Biro, R.; Tenne, R. *Solid State Sci.* **2000**, *2*, 663–672.
(20) Zak, A.; Feldman, Y.; Alperovich, V.; Rosentsveig, R.; Tenne, R. *J. Am. Chem. Soc.* **2000**, *122*, 11108–11116.
(21) Li, X.; Li, Y. D. *Chem.—Eur. J.* **2003**, *9*, 2726–2731.
(22) Rothschild; Tenne, R.; Sloan, J.; York, A. P. E.; Green, M. L. H.; Sloan, J.; Hutchison, J. L. *Chem. Commun.* **1999**, *36*, 3–364.
(23) Tsirlina, T.; Feldman, Y.; Homyonfer, M.; Sloan, J.; Hutchison, J. L.; Tenne, R. *Fullerene Sci. Technol.* **1998**, *6*, 157–165.
(24) Whitby, R. L. D.; Hsu, W. K.; Lee, T. H.; Boothroyd, C. B.; Kroto, H. W.; Walton, D. R. M. *Chem. Phys. Lett.* **2002**, *359*, 68–76.
(25) Coleman, K. S.; Sloan, J.; Hanson, N. A.; Brown, G.; Clancy, G. P.; Terrones, M.; Terrones, H.; Green, M. L. H. *J. Am. Chem. Soc.* **2002**, *124*, 11580–11581.
(26) Margolin, R.; Popovitz-Biro, A.; Albu-Yaron, A.; Moshkovich, L.; Rapoport; Tenne, R. *Curr. Nanosci.* **2005**, *1*, 253–262.
(27) Schuffenhauer, C.; Popovitz-Biro, R.; Tenne, R. *J. Mater. Chem.* **2002**, *12*, 1587–1591.
(28) Lee, G. H.; Jeong, J. W.; Huh, S. H.; Kim, S. H.; Choi, B. J.; Kim, Y. W. Y. W. *Int. J. Mod. Phys. B* **2003**, *17*, 1134–1140.
(29) Zelenski, C. M.; Dorhout, P. K. *J. Am. Chem. Soc.* **1998**, *120*, 734–742.
(30) Chen, S. L.; Li, F.; Gao; Tao, Z. L. *Chem. Mater.* **2003**, *15*, 1012–1015.
(31) Nath, M.; Rao, C. N. R. *Chem. Commun.* **2001**, *223*, 6–2237.
(32) Nath, M.; Kar, S.; Raychaudhuri, A. K.; Rao, C. N. R. *Chem. Phys. Lett.* **2003**, *368*, 690–695.
(33) Remskar, M.; Mrzel, A.; Skraba, Z.; Jesih, A.; Ceh, M.; Demsar, J.; Stadelmann, P.; Levy; Mihailovic, D. *Science* **2001**, *292*, 479–482.
(34) Remskar, M.; Skraba, Z.; Regula, M.; Ballif, C.; Sanjines, R.; Levy, F. *Adv. Mater.* **1998**, *10*, 246–249.
(35) ; Parilla, P. A.; Dillon, A. C.; Parkinson, B. A.; Jones, K. M.; Alleman, J.; Riker, G.; Ginley, D. S.; Heben, M. J. *J. Phys. Chem. B* **2004**, *108*, 6197–6207.
(36) Hacohen, Y. R.; Popovitz-Biro, R. Y.; Prior, Y.; Gemming, S.; Seifert, G.; Tenne, R. *Phys. Chem. Chem. Phys.* **2003**, *5*, 1644–1651.
(37) Sen, R.; Govindaraj, A.; Suenaga, K.; Suzuki, S.; Kataura, H.; Iijima, S.; Achiba, Y. *Chem. Phys. Lett.* **2001**, *340*, 242–248.
(38) Schuffenhauer, C.; Parkinson, B. A.; Jin-Phillipp, N. Y.; Joly-Pottuz, J.; Martin, J. M.; Popovitz-Biro, R.; Tenne, R. *Small* **2005**, *1*, 1100–1109.
(39) Vollath, D.; Szabo, D. V. *Mater. Lett.* **1998**, *35*, 236–244.
(40) Vollath, D.; Szabo, D. V. *Acta Mater.* **2000**, *48*, 953–957.
(41) Li, X J.; Ge; Li, Y. D. *Chem.—Eur. J.* **2004**, *10*, 6163–6171.
(42) Deegan, R. D.; Bakajin, O.; Dupont, T. F.; Huber, G.; Nagel, S. R.; Witten, *Nature* **1997**, *389*, 827–829.
(43) Loges, N.; Therese, H. A.; Graf, K.; Nasdala; Tremel, L. W. *Langmuir* **2006**, *22*, 3073–3080.
(44) Etzkorn, J.; Therese, H. A.; Rocker, F. N.; Zink, U.; Kolb, U.; Tremel, W. *Adv. Mater.* **2005**, *17*, 2372–2375.
(45) (a) Lightstone, J. M.; Patterson, M. J.; White, M. G. *Chem. Phys. Lett.* **2005**, *413*, 429–433. (b) Bertram, N.; Kim, Y. D.; Ganteför, G.; Sun, Q.; Jena, P.; Tamuliene, J.; Seifert, G. *Chem. Phys. Lett.* **2004**, *396*, 341–345. (c) For molecular examples see: Tremel, W.; Hoffmann, R.; Kertesz, M. *J. Am. Chem. Soc.* **1989**, *111*, 2030–2039. (d) Tremel, W.; Hoffmann, R.; Jemmis, E. D. *Inorg. Chem.* **1989**, *28*, 1213–24. (e) Bolle, U.; Tremel, W. *J. Chem. Soc., Chem. Commun.* **1994**, *217*, 19.

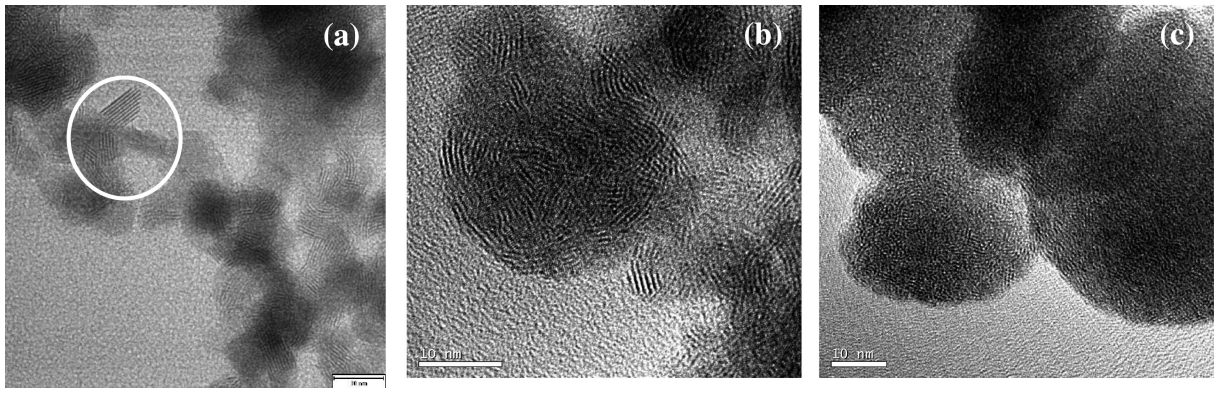

Figure 2. Typical HRTEM images of the precursor samples obtained at (a) 650, (b) 750, and (c) 850 °C. The scale bar in (a) is 20 nm. Whiskerlike particles (marked in (a)) are obtained in minor amounts for temperatures <750 °C.

Scheme 1. Hot Growth Zone around the Graphite Receptor (brown dotted line represents the minimum temperature required for particle growth)

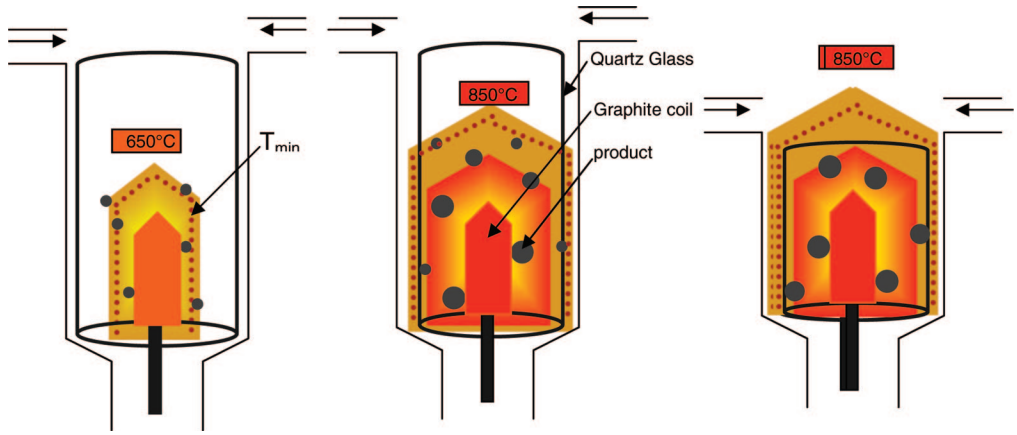

chosen in such a way that both reactants reached their final temperature in about the same time in order to provide a homogeneous reaction mixture for the whole duration of the experiment. The possibility of fast heating/cooling of the reaction zone makes this induction heated setup advantageous as compared to a slow tube furnace because "quenching" of the reaction is possible at any time. This allowed us to monitor the structure of the reaction products as a function of the reaction time by taking samples after given time intervals.

Thermal Annealing. Unless otherwise noted, annealing of the samples was done by taking the sample from the MOCVD setup in a corundum boat and placing it in the middle of the horizontal tube furnace at the specified temperature with a heating rate of 5 °C per min under constant argon gas flow of 100 sccm for 1 h.

Electron Microscopy. The products were characterized using high-resolution scanning electron microscopy (HRSEM) (LEO 1530 Field emission SEM, 6 kV extraction voltage). Transmission electron microscopy (TEM) was carried out on a Philips EM420 instrument with a twin lens and a Philips CM12 with a twin lens at an acceleration voltage of 120 kV. High-resolution images were taken with a Philips FEI TECNAI F30 ST electron microscope (field-emission gun, 300 kV extraction voltage) equipped with an Oxford EDX (energy-dispersive X-ray) spectrometer with a Si/Li detector and an ultrathin window for elemental analysis. Samples for TEM measurements were prepared from ethanolic suspensions of the samples. Three drops of the ultrasonicated suspension were administered on a Cu grid coated with FORMVAR polymer and an amorphous carbon layer.

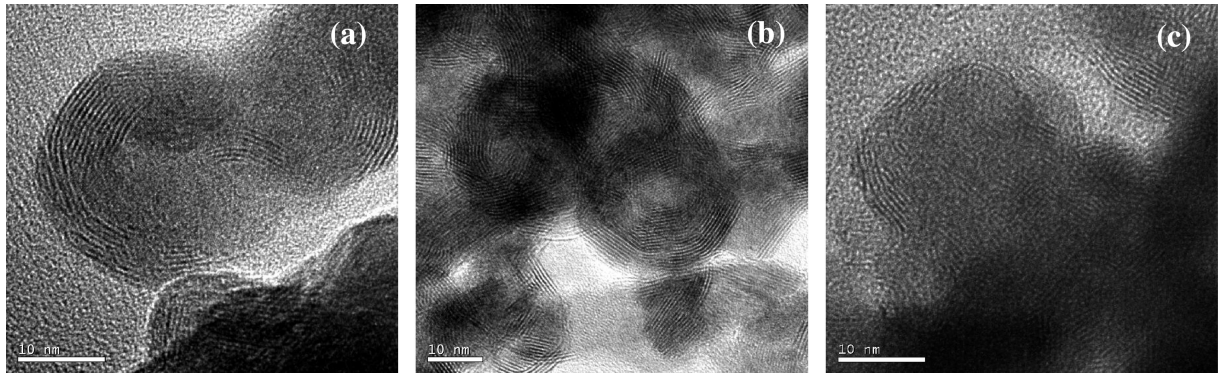

Figure 3. Typical HRTEM images of product particles after annealing of the precursor particles obtained at (a) 650,(b) 750 , and (c) 850 °C for 1 h at 800 °C.

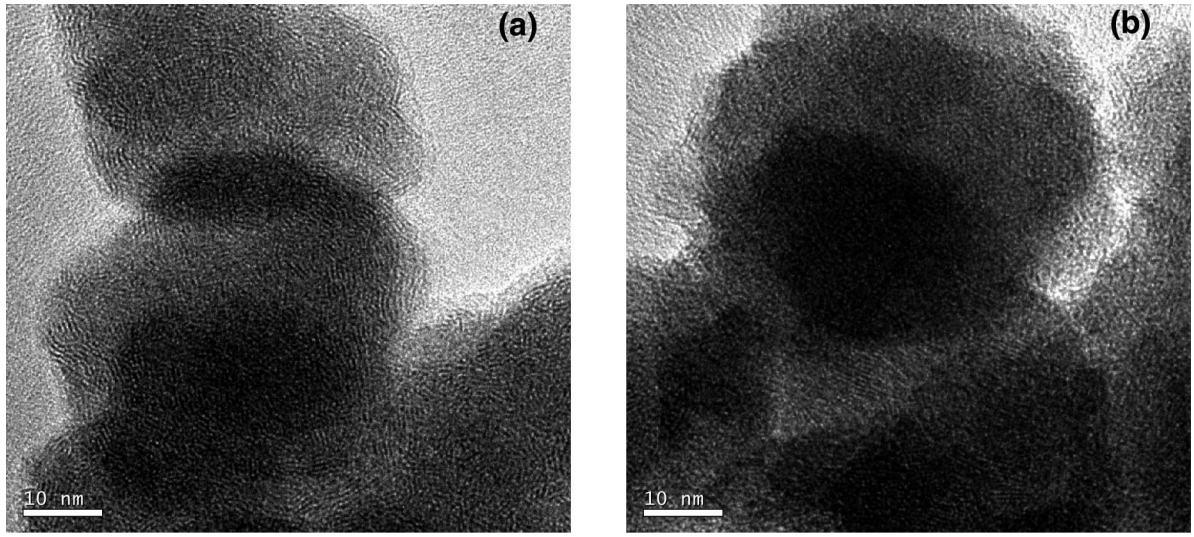

Figure 4. Typical HRTEM images of samples obtained at a reactor temperature of (a) 750 and (b) 850 °C before annealing.

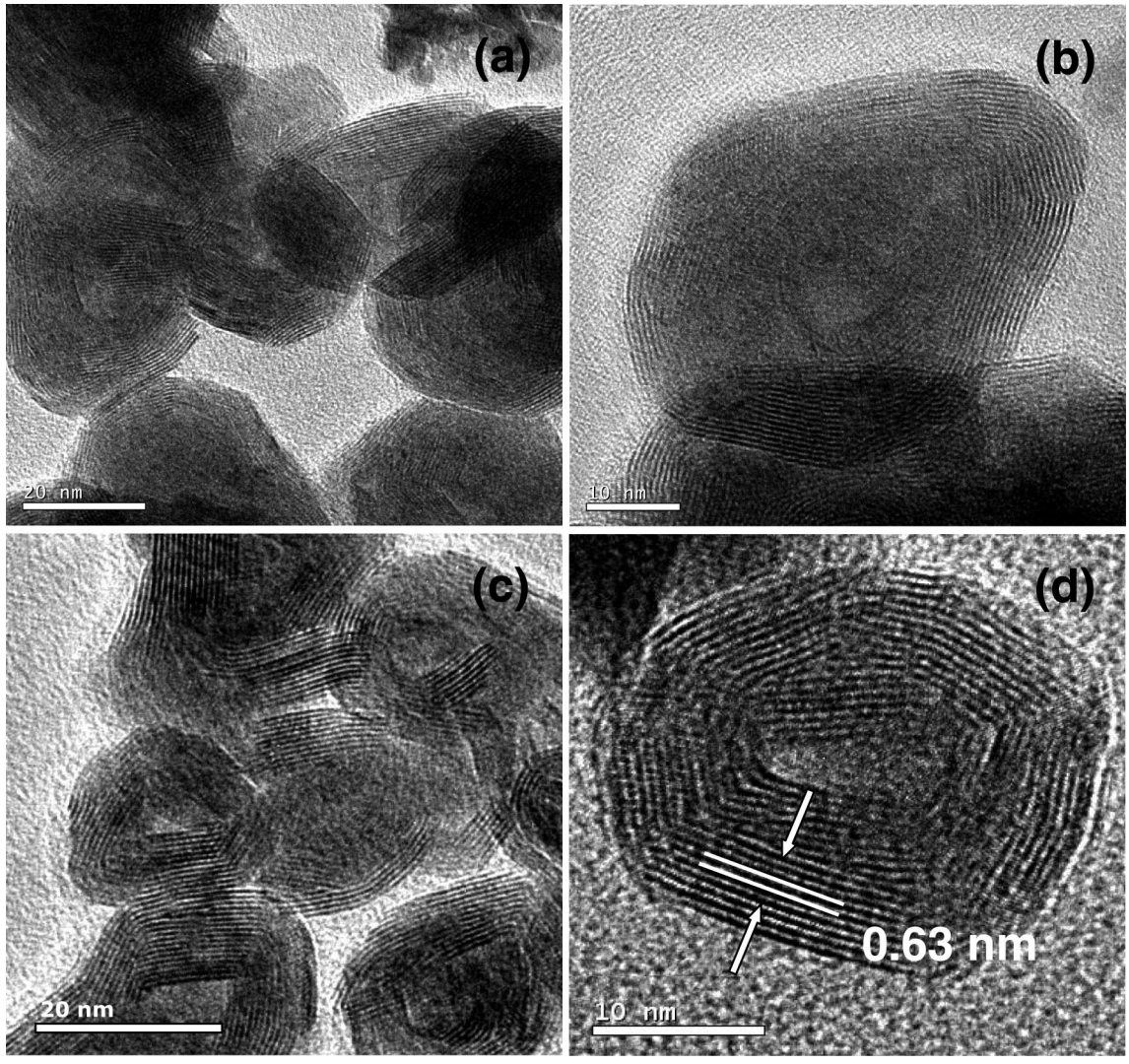

Figure 5. TEM overview (a, c) and HRTEM (b, d) images of samples obtained at 750 °C (a, c) and 850 °C (b, d) after annealing in a tube furnace at 900 °C for 1 h.

Results and Discussion

The synthesis of the ReS_2 nanoparticles was carried out according to the gross equation

$$Re_2(CO)_{10} + 2S \rightarrow 2ReS_2 + 10CO$$

The above equation describes the stoichiometric outcome of the reaction. It is highly probable that metal sulfide-carbonyl

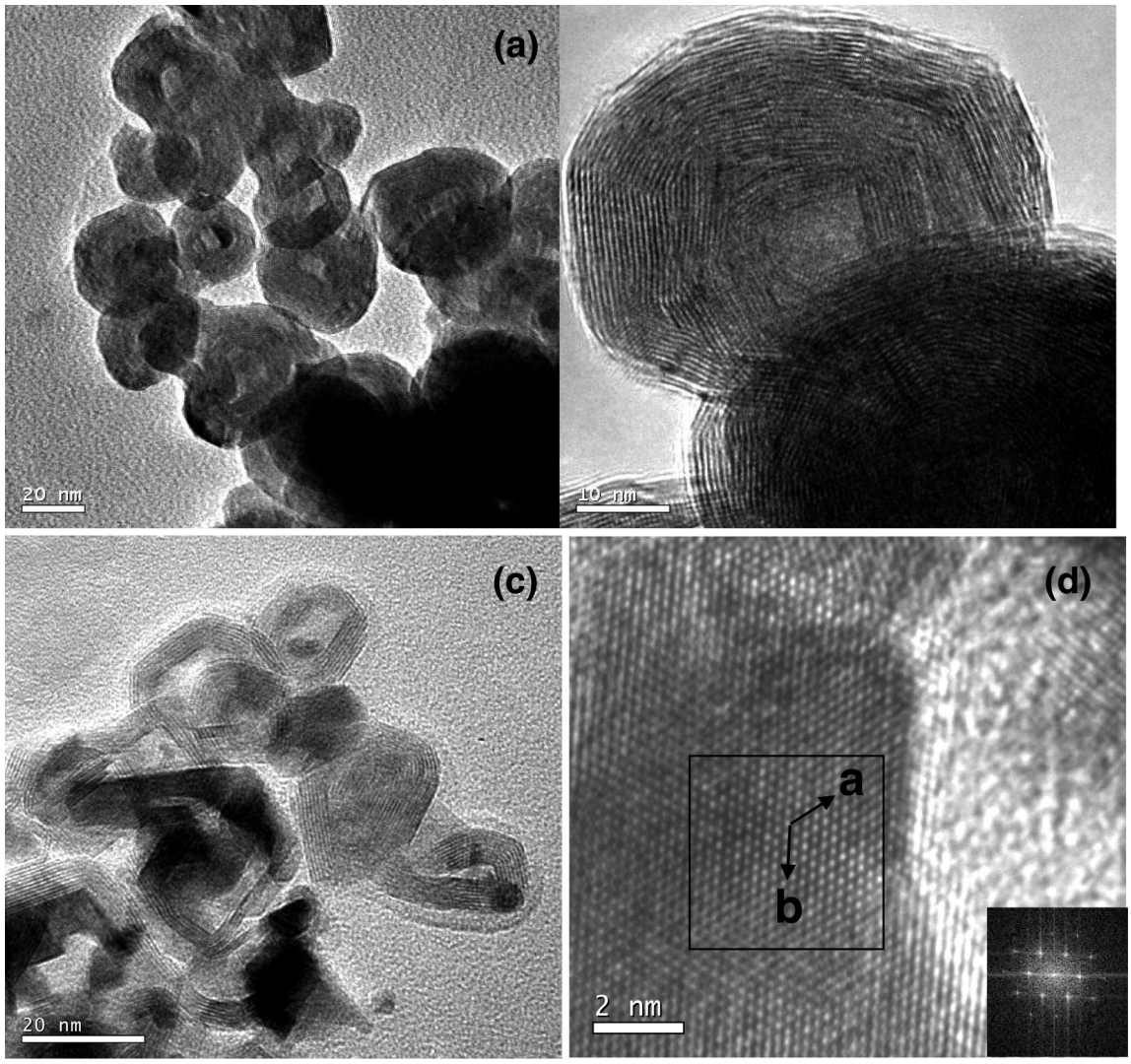

Figure 6. HRTEM images of a sample obtained at 850 °C (reactor temperature) followed by annealing at 900 °C for 5 h (a, b) and 30 min (c). (d) High-resolution image of the Re core from a IF-ReS_2 particle (shown in a and b) obtained after annealing for 5 h. The basis vectors *a* and *b* are marked by arrows. The inset in (d) shows the fast Fourier transform (FFT) of the region marked in (d).

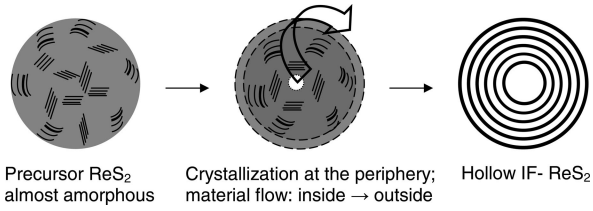

Figure 7. Formation of a hollow IF-ReS_2 nanoparticle from an amorphous Re−S mixture.

species appear as reaction intermediates.[46] The identification and characterization of these intermediates is a matter of ongoing research. The synthesis of onion-type ReS_2 nanoparticles was carried out in a two-step process, and the experimental conditions that have been used will be discussed briefly. In the first step, an amorphous intermediate was formed. Particle diameters are typically in a range between 10 and 60 nm. Variable parameters of this MOCVD step are mainly the temperature of the graphite receptor, the duration of stay of the particles in the growth zone, the carrier gas flow, and the reaction time. Carrier gas (argon) flow and reaction time turned out to have only a minor role in the formation of the IF-ReS_2, whereas the temperature of the graphite receptor turned out to play a key role as reported before for IF-MoS_2 particles.[45] The reaction intermediate was collected and annealed in the subsequent reaction step. During the annealing step, the amorphous precursor particles transform to IF-ReS_2.

Role of Temperature of the Graphite Receptor on the Morphology of the Reaction Intermediate. The synthesis of IF-ReS_2 particles was attempted at different temperatures between 650 and 850 °C in steps of 100 °C. The MOCVD reaction of $Re_2(CO)_{10}$ and S at temperatures between 650 and 850 °C (reaction time: 2 h) resulted in the deposition of a black soot which could easily be collected. The HRSEM images (Figure S1, Supporting Information) show that the MOCVD samples contain nanoparticles of unique morphology. The morphology of the samples was studied further by transmission electron microscopy (TEM) and also by X-Ray powder diffraction in order to obtain information about the bulk composition and the structure of the samples. Representative diffractograms of the products are shown in Figure 1. From the X-ray powder data, it can be concluded that the sample obtained at 550 °C mainly consists of elemental Re and a minor amount of ReS_2, which

is evident from the (002) reflection. Reflection profile broadening due to very small crystallite sizes and strong texture effects made a quantitative evaluation of these data by means of Rietveld refinements. XRD patterns of samples obtained at 650 and 750 °C, respectively, were refined using the crystal structure model of ReS_2-*aP*24.[47]

The results of the Rietveld refinements point to small crystallite sizes of 2.9 and 3.8 nm and a slight expansion along the stacking direction [001] of 0.4 and 1.8% for the samples prepared at 650 and 750 °C, respectively.

As spherical particle morphologies are more stable than isolated lamella-like structures at higher temperatures, the influence of the temperature on the primary products of the MOCVD reaction was studied. The temperature range between 650−850 °C proved to be most relevant. The primary samples obtained at 650 to 850 °C were highly disordered. Figure 2 shows typical HRTEM images of the precursor samples obtained at (a) 650, (b) 750, and (c) 850 °C. At 650 °C, two different types of particles, (i) well-ordered whiskerlike particles with few ReS_2 layers and particle diameters of about 3−5 nm and (ii) disordered and mostly amorphous round particles with diameters of 20−30 nm, were obtained in about equal quantities. At 750 °C, curved, disordered round particles with diameters of 20−30 nm were obtained in significantly higher quantities than the whiskerlike particles. At 850 °C, round particles with diameters ranging from 10 to 60 nm were obtained. In general, the crystallinity of the particles increased with increasing temperature of the graphite receptor (see Scheme 1).

Subsequently, the primary products obtained at 650−850 °C were collected and annealed at 800 °C for 1 h under argon in a tube furnace. In Figure 3, we show HRTEM images of the precursor samples synthesized at (a) 650, (b) 750, and (c) 850 °C annealed at 800 °C for 1 h.

Thermal annealing of the sample led to an increase in long-range order. A large quantity of closed and open onion-type ReS_2 particles with diameters between 20 and 40 nm were formed during the heat treatment. During the annealing process, the amorphous spherical particles transformed into facetted onion-type particles. However, the ratio of small whiskerlike particles and larger onion-type particles after annealing is almost equal to the ratio of the bigger and smaller sized particles before annealing (small whisker-like particles are shown in Figure S2 of the Supporting Information).

Role of Duration of Stay of the Particles in the Growth Zone on the Morphology of the Precursor Particles. To reduce the size distribution of the particles, the temperature of the reactor (i.e., of the growth zone) has to be increased or the volume of the growth region has to be reduced in order to level the trajectories of the individual particles. As a variation of the reactor temperature did not lead to the desired results, the dimensions of the reactor were adjusted by reducing its length by a factor of 2. Initially, the length of the growth region between the gas inlet and the graphite receptor (see Figure S3 in the Supporting Information) was approximately 30 cm, and it was reduced to 15 cm in the modified reactor layout.

This change of the reactor setup sharpened the size distribution and improved the morphology of the product considerably. The resulting IF-ReS_2 particles had diameters ranging from 20 to 50 nm. Only round particles were obtained, but the layers were highly disordered. Figure 4 shows HRTEM images of the ReS_2 precursor samples obtained at 750 and 850 °C. Samples obtained in the modified MOCVD setup were annealed subsequently at 900 °C for 1 h in order to achieve transformation to IF-ReS_2. The corresponding TEM images in Figure 5 indicate that products contained exclusively hollow IF-ReS_2 particles with diameters ranging from 20 to 50 nm.

Samples obtained at 850 °C and annealed for 1 h at 900 °C contained a core of elemental rhenium (Figure S4, Supporting Information). To probe whether the Re core is formed during the nucleation process or by thermal decomposition of IF-ReS_2 during the annealing step, the annealing time was increased from 1 to 5 h at 900 °C. The annealing time of the precursor turned to play an important role in the composition of resulting IF-ReS_2 particles. Extended annealing resulted in the thermal decomposition of IF-ReS_2 and a concomitant elimination of sulfur from the IF-ReS_2 particles (Figure 6). As ReS_2 is the most metal-rich binary Re−S phase, elemental Re is segregated and Re and ReS_2 are formed as neighboring phases of the Re−S phase diagram.

As sulfur is known to permeate metal sulfides,[21] the annealing experiments were also carried out in the presence of sulfur vapor during in the annealing step. However, no significant change in the particle structure and composition was observed.

Mechanism of the Hollow Particle Formation. Conceptually, the formation of solid-state compounds can be broken down into two key steps: the interdiffusion of the reactants and the nucleation and crystallization of the products. Because IF-ReS_2 represents a binary nonequilibrium phase, the synthetic goal is to gain kinetic control of the reaction by eliminating diffusion as a rate-limiting step. This leaves nucleation as the crucial reaction step associated. A homogeneous, amorphous mixture of the components is a suitable reaction intermediate. The interdiffusion of the reactants is driven by the mixing enthalpy; only the formation of the amorphous mixture is diffusion-controlled. For particles with diameters as small as 10−20 nm diffusion is complete after formation. As a result, nucleation becomes the rate-limiting step in the formation of the ordered "crystalline" solid (IF-ReS_2). When the amorphous particles are heated, ReS_2 starts to nucleate and grow until its growth exhausts one of the reactants within the particle volume or until the particle

(46) (a) Wildervanck, J. C.; Jellinek, F. *J. Less-Common Met.* **1971**, *24*, 73–81. (b) Alcock, N. W.; Kjekshus, A. *Acta Chem. Scand.* **1965**, *19*, 79–94. (c) Coleman, K. S.; Sloan, J.; Hanson, N. A.; Brown, G.; P.Clancy, G. P.; Terrones, M.; Terrones, H.; Green, M. L. H. *J. Am. Chem. Soc.* **2002**, *124*, 11581–11582, The linewidth of the diffraction data given in the supporting information of this reference indicates the main product not to be IF-ReS_2.

(47) Smigelsklas, A. D.; Kirkendall, E. O. *Trans AIME* **1947**, *171*, 130–142.

boundary is reached (see Figure 7). Because intraparticle growth is preferred over interparticle growth, a size restriction is imposed by the diameter of the particles containing the amorphous mixture.

The transformation from the amorphous precursor particle to IF-ReS_2 starts at the particle boundary, where the surface energy and reactivity is highest, and an ordered ReS_2 shell is formed around the still amorphous core. As a result, nucleation and crystal growth of the new solid phase proceed outside-in. As the density of the "crystalline" IF-ReS_2 is larger than that of the amorphous core, there is a net mass transfer to the particle boundary, whereas the interior of the particle is depleted. The driving force for the mass transfer is a concentration gradient of ReS_2 due to the compactization. After a shell consisting of 10−20 ReS_2 layers has formed, the material flow from the interior of the particle to the rim ceases. As a result, hollow particles are formed.

These experiments demonstrate that the transformation of an amorphous precursor particle to a "crystalline" ordered phase can provide an effective synthetic route to controlling the particle morphology. The spherical shape of the amorphous precursor is imposed by the minimization of its interfacial energy. The mechanism of the hollow particle formation by the transformation from an amorphous to a more dense crystalline material may be viewed as the 3D analogue of the so-called coffee-stain effect (where ringlike deposits are obtained on a 2D support upon evaporation of a solvent drop),[43,44] which is related to the Kirkendall effect.[47] An outward flow of material in the crystallizing spherical particle is produced when the outer particle boundary is pinned so that material compacting at the rim of the sphere must be replenished by a mass flow from the interior. This flow is capable of transferring 100% of the precursor particles to the sphere boundary and thus accounts for the formation of a hollow sphere.

Conclusions

In summary, we have demonstrated a new and simple synthetic approach to hollow nested fullerene-like IF-ReS_2 nanoparticles, which are difficult to obtain by other methods such as the sulfidization of the corresponding metal oxide, ReO_2. In the first reaction step, amorphous nanoparticles of layered ReS_2 are formed from gaseous precursors. This MOCVD approach allows for short reaction times, facile control of the reaction process, and high purity products; it also opens opportunities to monitor the particle growth by gas phase analytical methods such as mass spectrometry and to kinetically control the growth process by a proper choice of the experimental conditions. In a second subsequent reaction step, annealing in an argon atmosphere, the resulting amorphous nanoparticles are allowed to "crystallize" to form nested fullerene-type structures. The formation of hollow IF-like ReS_2 particles from closed spheres of an amorphous precursor is analogous to the formation of void space in metals or intermetallic compounds due to the Kirkendall-effect known from metallurgy.

This simple and inexpensive approach may be scaled easily and allows the synthesis of nanostructured ReS_2 in large quantities. There are further prospects to further analyze the solid-state transformation of the primary ReS_2 particles into IF-ReS_2 by using in situ heating NMR and TEM studies. Experiments toward this goal are in progress.

Acknowledgment. This research was supported by a fellowship to A.Y. from POLYMAT, the Graduate School of Excellence of the State of Rhineland-Palatinate. We are indebted to the Center for Electron Microscopy (EZMZ) for access to its facilities and the Materials Science Center (MWFZ) in Mainz for support.

Supporting Information Available: A HRSEM image of the ReS_2 nanoparticles obtained from the MOCVD process at 750 °C (Figure S1); HRTEM image of whiskerlike Re nanoparticles (Figure S2); schemes of the reactor setup (Figure S3); HRTEM image of an IF-ReS_2 particle with a Re core (Figure S4) (PDF). This material is available free of charge via the Internet at http://pubs.acs.org.

CM7030619